Hydrodynamic forces and critical stresses in low-density aggregates under shear flow

-

Supplementary Information

Marco Vanni, Andrea Gastaldi

1 Non-dimensional form of the solution

All terms of the mobility matrix can be expressed as:

$$\mathbf{m}_{i,j}^{\eta} = \frac{\bar{\mathbf{m}}_{i,j}^{\eta}}{\mu a^{q}} \tag{1}$$

and $q = 1$ for $\eta = UF$, $q = 2$ for $\eta = UC$ and $\eta = \Omega F$, $q = 3$ for $\eta = \Omega C$, while the dimensionless term $\bar{\mathbf{m}}_{i,j}^{\eta}$ depends only on the non-dimensional geometric configuration of the system [Durlofsky et al., 1987]. Then, by dividing all terms of Eq. (8) of the main paper by $\dot{\gamma}$ and substituting the previous relationship one obtains:

$$\left[\begin{array}{ccc|ccc|cc} \bar{\mathbf{m}}_{1,1}^{UF} & \cdots & \bar{\mathbf{m}}_{1,n_p}^{UF} & \bar{\mathbf{m}}_{1,1}^{UC} & \cdots & \bar{\mathbf{m}}_{2,n_p}^{UC} & \mathbf{I} & \boldsymbol{\alpha}_1/a \\ \cdots & \cdots & \cdots & \cdots & \cdots & \cdots & \cdots & \cdots \\ \bar{\mathbf{m}}_{n_p,1}^{UF} & \cdots & \bar{\mathbf{m}}_{n_p,n_p}^{UF} & \bar{\mathbf{m}}_{n_p,1}^{UC} & \cdots & \bar{\mathbf{m}}_{n_p,n_p}^{UC} & \mathbf{I} & \boldsymbol{\alpha}_{n_p}/a \\ \hline \bar{\mathbf{m}}_{1,1}^{\Omega F} & \cdots & \bar{\mathbf{m}}_{1,n_p}^{\Omega F} & \bar{\mathbf{m}}_{1,1}^{\Omega C} & \cdots & \bar{\mathbf{m}}_{2,n_p}^{\Omega C} & \mathbf{0} & \mathbf{I} \\ \cdots & \cdots & \cdots & \cdots & \cdots & \cdots & \cdots & \cdots \\ \bar{\mathbf{m}}_{n_p,1}^{\Omega F} & \cdots & \bar{\mathbf{m}}_{n_p,n_p}^{\Omega F} & \bar{\mathbf{m}}_{n_p,1}^{\Omega C} & \cdots & \bar{\mathbf{m}}_{n_p,n_p}^{\Omega C} & \mathbf{0} & \mathbf{I} \\ \hline \mathbf{I} & \cdots & \mathbf{I} & \mathbf{0} & \cdots & \mathbf{0} & \mathbf{0} & \mathbf{0} \\ \boldsymbol{\alpha}_1^T/a & \cdots & \boldsymbol{\alpha}_{n_p}^T/a & \mathbf{I} & \cdots & \mathbf{I} & \mathbf{0} & \mathbf{0} \end{array}\right] \left\{\begin{array}{c} \mathbf{f}_1^H/(\mu\dot{\gamma}a^2) \\ \cdots \\ \mathbf{f}_{n_p}^H/(\mu\dot{\gamma}a^2) \\ \hline \mathbf{c}_1^H/(\mu\dot{\gamma}a^3) \\ \cdots \\ \mathbf{c}_{n_p}^H/(\mu\dot{\gamma}a^3) \\ \hline \mathbf{u}_{cm}/(\dot{\gamma}a) \\ \boldsymbol{\omega}_{cm}/\dot{\gamma} \end{array}\right\} = \left\{\begin{array}{c} \mathbf{u}^{\infty}(\mathbf{x}_1)/\dot{\gamma}a \\ \cdots \\ \mathbf{u}^{\infty}(\mathbf{x}_{n_p})/\dot{\gamma}a \\ \hline \boldsymbol{\omega}^{\infty}(\mathbf{x}_1)/\dot{\gamma} \\ \cdots \\ \boldsymbol{\omega}^{\infty}(\mathbf{x}_{n_p})/\dot{\gamma} \\ \hline \mathbf{0} \\ \mathbf{0} \end{array}\right\} \tag{2}$$

The matrix and the right hand side vector depend only on the non-dimensional geometric configuration (remember that $\mathbf{u}^{\infty}(\mathbf{x}_i)/\dot{\gamma}a = (z_i/a, 0, 0)^T$ and $\boldsymbol{\omega}^{\infty}(\mathbf{x}_i)/\dot{\gamma} = (0, 1/2, 0)^T$). Consequently the vector of unknowns, too, must be a function only of the non-dimensional geometry of the system and therefore it is the same for all geometrically similar configurations.

2 Evaluation of internal forces: the case of a simple aggregate

As an example of application of the method presented in the paper, we examine the pentamer shown in Fig. 1, subjected to the external hydrodynamic forces $\mathbf{f}_i^H$

and to the external hydrodynamic torques $\mathbf{c}_i^H$ acting on each single monomer i. In addition each monomer exchanges internal forces and torques with its neighbours. For instance, as detailed in the right part of Fig. 1, monomer 4 is subjected to internal interactions due to the actions of monomer 2 ($\mathbf{F}_{24}$ and $\mathbf{C}_{24}$) and monomer 5 ($\mathbf{F}_{54}$ and $\mathbf{C}_{54}$). Consequently, the balance of forces on monomer 4 is:

$$\mathbf{f}_4^H + \mathbf{F}_{24} + \mathbf{F}_{54} = 0 \tag{3}$$

where $\mathbf{f}_4^H$ is known from the Stokesian dynamics solution. Similar balances can be written for the other monomers, resulting in:

$$\begin{array}{l} \mathbf{f}_1^H + \mathbf{F}_{21} = 0 \\ \mathbf{f}_2^H + \mathbf{F}_{12} + \mathbf{F}_{32} + \mathbf{F}_{42} = 0 \\ \mathbf{f}_3^H + \mathbf{F}_{23} = 0 \\ \mathbf{f}_4^H + \mathbf{F}_{24} + \mathbf{F}_{54} = 0 \\ \mathbf{f}_5^H + \mathbf{F}_{45} = 0 \end{array} \tag{4}$$

By the action-reaction law we have $\mathbf{F}_{i,j} = -\mathbf{F}_{j,i}$ and hence we can remove four of the unknowns from the above equations. In addition, due to the prescribed mechanical equilibrium of the aggregate, the last equation is redundant and can be deleted. Therefore we are left with an algebraic system of 4 (=n_p-1) vectorial equations in the four unknowns $\mathbf{F}_{12}$, $\mathbf{F}_{23}$, $\mathbf{F}_{24}$, $\mathbf{F}_{45}$.

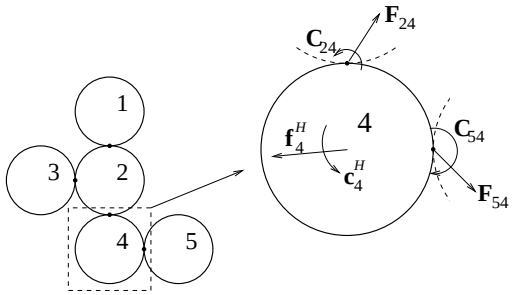

Figure 1: Internal and external forces and torques acting on a monomer belonging to a pentamer.

Internal moments are evaluated similarly. The balances of moment for each monomer of our pentamer are:

$$\begin{array}{l} \mathbf{c}_1^H + \mathbf{C}_{21} + \frac{\mathbf{x}_2-\mathbf{x}_1}{2} \times \mathbf{F}_{21} = 0 \\ \mathbf{c}_2^H + \mathbf{C}_{12} + \mathbf{C}_{32} + \mathbf{C}_{42} + \frac{\mathbf{x}_1-\mathbf{x}_2}{2} \times \mathbf{F}_{12} + \frac{\mathbf{x}_3-\mathbf{x}_2}{2} \times \mathbf{F}_{32} + \frac{\mathbf{x}_4-\mathbf{x}_2}{2} \times \mathbf{F}_{42} = 0 \\ \mathbf{c}_3^H + \mathbf{C}_{23} + \frac{\mathbf{x}_2-\mathbf{x}_3}{2} \times \mathbf{F}_{23} = 0 \\ \mathbf{c}_4^H + \mathbf{C}_{24} + \mathbf{C}_{54} + \frac{\mathbf{x}_2-\mathbf{x}_4}{2} \times \mathbf{F}_{24} + \frac{\mathbf{x}_5-\mathbf{x}_4}{2} \times \mathbf{F}_{54} = 0 \\ \mathbf{c}_5^H + \mathbf{C}_{45} + \frac{\mathbf{x}_4-\mathbf{x}_5}{2} \times \mathbf{F}_{45} = 0 \end{array} \tag{5}$$

The hydrodynamic torques appearing in these equations are known from the Stokesian dynamics simulation, while the internal forces are given by the solution of the previous algebraic system. As before, the last equation is redundant and the action-reaction law implies $\mathbf{C}_{i,j} = -\mathbf{C}_{j,i}$. Therefore, in the end, we obtain again an easily solvable algebraic system of $(n_p - 1)$ vectorial equations in the $(n_p - 1)$ unknown internal torques $\mathbf{C}_{12}$, $\mathbf{C}_{23}$, $\mathbf{C}_{24}$, $\mathbf{C}_{45}$.

3 Validation of the method on test systems

3.1 Motion of the particles

In order to test the accuracy of the implemented method, we examined the case of a doublet of equal sized and contacting spheres positioned on the $x - z$ plane and immersed in a simple shear flow with prescribed velocity gradient $\dot{\gamma} = \frac{\mathrm{d}u_x^\infty}{\mathrm{d}z}$.

Nir and Acrivos [1973] analytically solved the more general problem of the motion of a sphere doublet (with each sphere of arbitrary size) in a linear shear field at creeping flow conditions. Applying their solution to our case, the angular velocity results [Derksen, 2008]:

$$\omega_y = \frac{1}{2}\dot{\gamma}\,[1 + k\cos(2\theta)] \tag{6}$$

where $k = 0.594$ for two equal sized touching spheres and the angle θ defines the orientation of the doublet in the plane $x - z$. Since the structure is symmetric and its center of mass is set on the vorticity axis (y) of the shear flow field, the doublet simply rotates on the $x - z$ plane and hence the other components of the angular velocity are null.

As apparent from Fig. 2, our Stokesian dynamics data agree well with the exact solution for the rotational velocity of the doublet (the largest error is about 1%). The velocity is a sinusoidal function of the orientation, having its maxima at $0, \pi, 2\pi$, when the axis of the doublet is perpendicular to the undisturbed fluid velocity, and minima at $\pi/2, 3\pi/2$, when it is aligned with the plane of null fluid velocity. The orientation-average value of ω_y is $\dot{\gamma}/2$, that is, the value at which a solid sphere rotates in a shear flow. The time-average value of ω_y for the doublet is instead smaller than $\dot{\gamma}/2$, because the doublet spends more time in the low velocity region of the curve than in the high velocity one. The dimensionless doublet rotation period estimated by our explicit time-integration technique is $\dot{\gamma}\, t_r = 15.45$, which compares well with the exact value of 15.62 [Adler et al., 1981] and is significantly larger that the value of 4π (=12.57) valid for a solid sphere rotating at the constant velocity of $\dot{\gamma}/2$.

To assess the accuracy of the time integration method we examined the dynamics of straight rigid chains of spheres of different length (from 3 to 10 monomers) in the same hydrodynamic configuration as the doublet. In all cases the estimated period of rotation agreed within 1-2% with the values reported in the literature [Zia

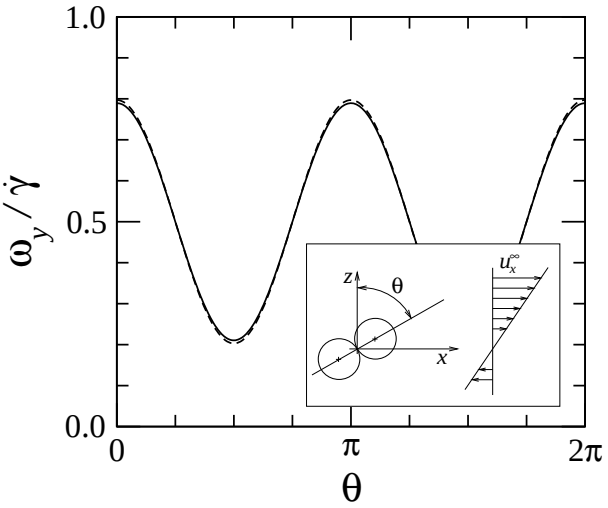

Figure 2: Angular velocity of a doublet versus orientation. Continuous line: Stokesian dynamics simulations; dashed line: exact analytical solution.

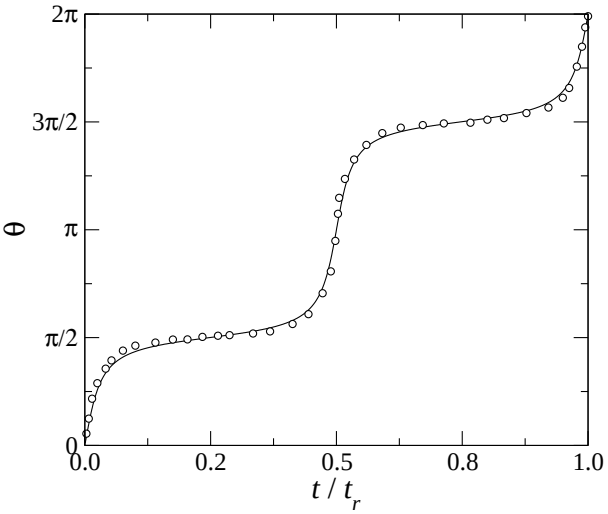

Figure 3: Orientation of a rod-like aggregate of 8 spheres versus dimensionless simulation time. Continuous line: Stokesian dynamics; circles: results by Karnis et al.Karnis et al. [1966].

et al., 1967] and also the instantaneous orientation is predicted accurately, as evidenced by Fig. 3, where the values of the angle θ formed by a chain of 8 spheres with the z-axis obtained by Stokesian dynamics are compared with the theoretical

ones [Karnis et al., 1966].

3.2 Stress distribution

According to the solution by Nir and Acrivos [1973] the interparticle normal and transverse forces acting on a doublet of equal sized touching spheres (i.e., the components of the interaction force between the spheres acting along and perpendicular to the line connecting the sphere centers) are:

$$N = \pi\mu\frac{a^2}{2}\dot{\gamma}\,(h_1 + h_2)\sin(2\theta) \tag{7}$$

$$T = \pi\mu\frac{a^2}{2}\dot{\gamma}h_1\cos(2\theta) \tag{8}$$

where h_1 and h_2 are respectively 4.463 and 7.767.

The solution is periodic over the interval π and, as it is shown in Fig. 4, a tensile force is obtained for θ between 0 and $\pi/2$, while the other orientations give compression. The extreme value is obtained at $\theta = \pi/4$ for traction, while it is located at $-\pi/4$ for compression. In this case the discrepancy between exact solution and

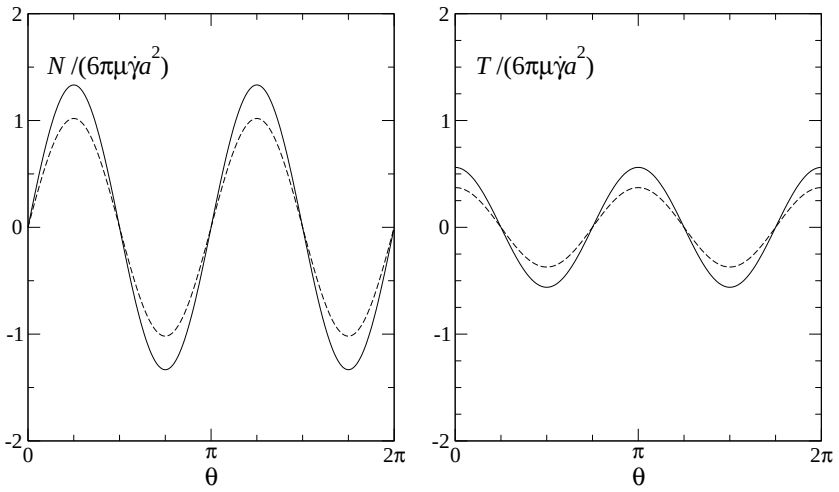

Figure 4: Normal and transverse forces at the inter-particle junction of a doublet versus orientation. Continuous line: Stokesian dynamics simulations; dashed line: exact analytical solution.

Considering that the FT-Stokesian dynamics method is based on a low order approximation of the mobility matrix, it is apparent that the deviations are due to the truncated higher order terms. However, it is interesting to notice that a global property such as the angular velocity is predicted much more accurately than the local interparticle interaction, probably because the combination of the terms of the

mobility matrix over the whole structure compensate for the error on the calculation of each one of them.

4 Rotation dynamics of aggregates

The rotation dynamics of our clusters can be summarised in two variables: the time-averaged angular velocity, $\bar{\omega}_y$, which determines the period of the oscillations, and the root mean square fluctuation of the angular velocity $\omega'_{y,\mathrm{rms}}$, which gives an indication of the amplitude of the oscillations. Fig. 5 shows the results and compares quantitatively PC and CC aggregates. The markers in the Figure represents the average response of each one of the studied groups of aggregates. The responses of aggregates with the same value of D_f and k_f but different n_p are very close and thus they are represented by a single marker in the graph.

Objects with perfect spherical symmetry have $\bar{\omega}_y = \dot{\gamma}/2$ and $\omega'_{y,\mathrm{rms}} = 0$, since their angular velocity is constant. Our aggregates show smaller average velocity and presence of fluctuations. Clearly the deviation from the spherical behavior is more intense the more disordered is the aggregate and hence it is small for PC systems and quite large for CC ones, and, in addition it increases with decreasing fractal dimension. The great variability among CC aggregates is reflected by the large standard deviations of $\bar{\omega}_y$ and $\omega'_{y,\mathrm{rms}}$ for each examined population.

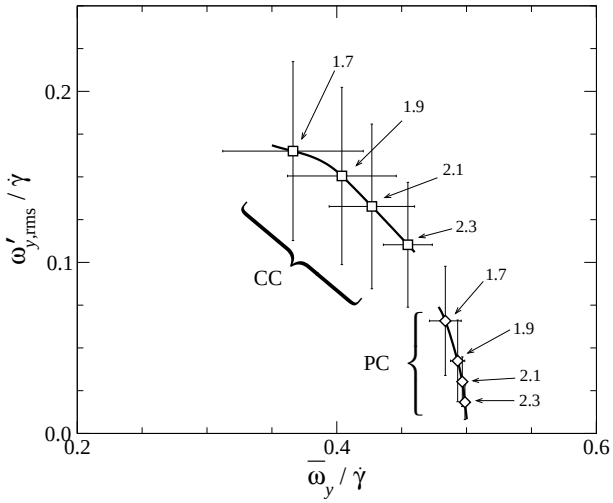

Figure 5: Average value and rms fluctuation of the angular velocity of families of aggregates of different fractal dimension in a shear flow.

References

P.M. Adler, H.L. Takamura, K. Goldsmith, and S.G. Mason. Particle motions in sheared suspensions. xxx. rotations of rigid and flexible dumbbells (theoretical). *J. Colloid Interface Sci.*, 83(2):502–515, 1981.

J.J. Derksen. Flow-induced forces in sphere doublets. *J. Fluid Mech.*, 608:337–356, 2008.

L. Durlofsky, J. F. Brady, and G. Bossis. Dynamic simulation of hydrodynamically interacting particles. *J. Fluid Mech.*, 180:21–49, 1987.

A. Karnis, H.L. Goldsmith, and S.G Mason. The flow of suspensions through tubes: V. inertial effects. *Can. J. Chem. Eng.*, 44(4):181–193, 1966.

A. Nir and A. Acrivos. On the creeping motion of two arbitrary-sized touching spheres in a linear shear field. *J. Fluid Mech.*, 59:209–223, 1973.

I.Y.Z. Zia, R.G. Cox, and S.G. Mason. *Proc. R. Soc. London, A*, 300:421–441, 1967.